

# Supersolid stripe crystal from finite-range interactions on a lattice

Guido Masella,<sup>1</sup> Adriano Angelone,<sup>2,3</sup> Fabio Mezzacapo,<sup>4,1</sup> Guido Pupillo,<sup>1</sup> and Nikolay V. Prokof'ev<sup>5,1</sup>

<sup>1</sup>*icFRC, IPCMS (UMR 7504) and ISIS (UMR 7006),*

*Université de Strasbourg and CNRS, 67000 Strasbourg, France*

<sup>2</sup>*Abdus Salam International Centre for Theoretical Physics, strada Costiera 11, 34151 Trieste, Italy*

<sup>3</sup>*SISSA, via Bonomea 265, 34136 Trieste, Italy*

<sup>4</sup>*Univ Lyon, Ens de Lyon, Univ Claude Bernard,*

*CNRS, Laboratoire de Physique, F-69342 Lyon, France*

<sup>5</sup>*Department of Physics, University of Massachusetts, Amherst, Massachusetts 01003, USA*

(Dated: September 20, 2019)

Strong, long-range interactions present a unique challenge for the theoretical investigation of quantum many-body lattice models, due to the generation of large numbers of competing states at low energy. Here, we investigate a class of extended bosonic Hubbard models with off-site terms interpolating between short- and infinite-range, thus allowing for an exact numerical solution for all interaction strengths. We predict a novel type of stripe crystal at strong coupling. Most interestingly, for intermediate interaction strengths we demonstrate that the stripes can turn superfluid, thus leading to a self-assembled array of quasi one-dimensional superfluids. These bosonic *superstripes* turn into an isotropic supersolid with decreasing the interaction strength. The mechanism for stripe formation is based on cluster self-assembly in the corresponding classical ground state, reminiscent of classical soft-matter models of polymers, different from recently proposed mechanisms for cold gases of alkali or dipolar magnetic atoms.

PACS numbers: 05.30.-d, 67.80.K-, 64.75.Yz

The effects of long-range interactions on quantum phases of many-body lattice systems is a hot topic of research [1–5], which is driven by outstanding advances in precision experiments with strongly interacting magnetic atoms [6–10], polar molecules [11, 12], Rydberg-excited atoms [13, 14], ions [15–18], and neutral atoms coupled to photonic modes [19–24]. For bosonic particles, exact numerical results from quantum Monte-Carlo methods can in principle predict thermodynamic properties of any unfrustrated model. However, long-range interactions in combination with confinement to periodic potentials present a unique challenge as they generate a proliferation of metastable low-energy states, whose number exponentially increases with the system size [25, 26], even in the absence of external frustration. This usually results in, e.g., devil’s staircase-type structures that are essentially intractable [27–30].

Much interest was recently generated by the demonstration of stripe behavior in spin-orbit-coupled Bose-Einstein condensates [31–35] as well as droplet formation in clouds of dipolar magnetic atoms in the mean-field regime [36–38], due to a competition of quantum fluctuations, short- and long-range interactions [37, 39, 40]. Exact numerical results have further demonstrated theoretically that anisotropic dipolar interactions for particles confined to two dimensions (2D) can generate stripe behavior while preserving superfluidity [41, 42], corresponding to a possible realization of so-called stripe supersolidity [43, 44]. The latter has a long history in quantum condensed matter, where it was first introduced as *superstripe* phase, in that non-homogeneous metallic structures with broken spatial symmetry were found to favor

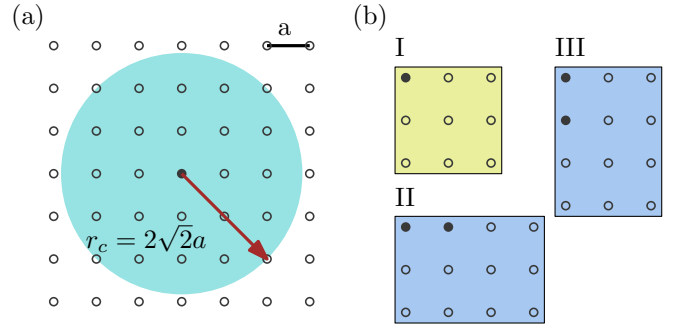


FIG. 1. Sketch of the interaction potential chosen in our work on a square lattice of spacing  $a$  [panel (a)]. The shaded region indicates the interaction range, which extends up to the critical radius  $r_c = 2\sqrt{2}a$ . In the large- $V$  limit, the GS of model Eq. (1) at our chosen density  $\rho = 5/36$  can be found by tiling the lattice with clusters of type I, II and III [panel (b)]. Empty and full circles refer to empty and occupied lattice sites, respectively.

superconductivity [45]. While the microscopic origin of such a phase is still a subject of debate, it is clear that a key role is played by a combination of strong interactions and the lattice potential. In this context, key open challenges are to propose and understand basic mechanisms for (super)stripe formation on lattice geometries of experimental interest and to provide exact theoretical predictions in the regime of strong interactions.

In this work, we study the low temperature phase diagram of an ensemble of bosonic particles confined to a square lattice geometry and interacting via a soft-shoulder potential. The latter has a finite range that

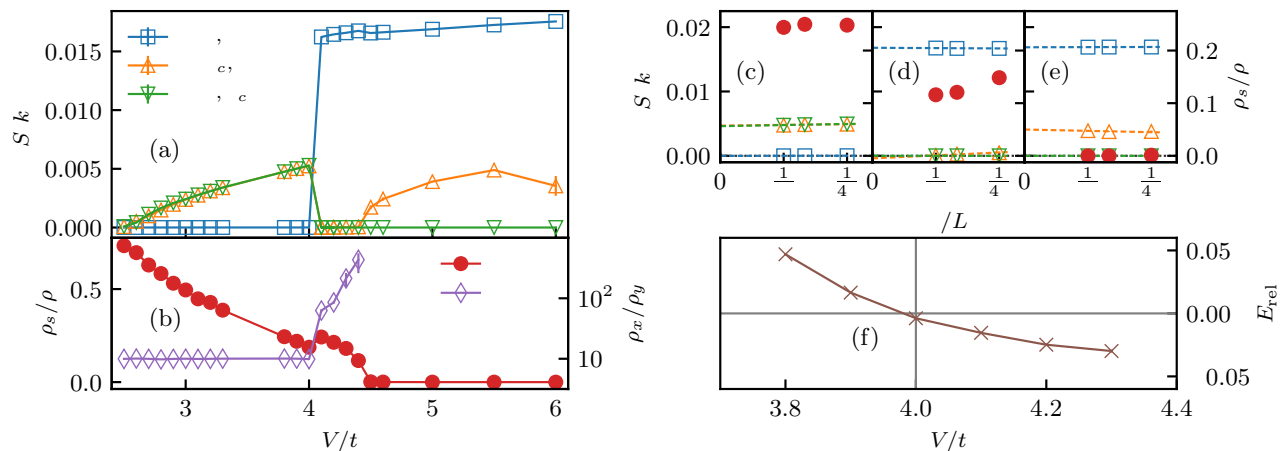


FIG. 2. Panel (a): Structure factor  $S(\mathbf{k})$  as a function of  $V/t$  for values of lattice wave vector  $\mathbf{k} = (k_c, 0)$  (up-pointing triangles),  $(0, k_c)$  (down-pointing triangles),  $(0, k_s)$  (squares) characteristic of the IS, SC, and SS ordered phase, respectively (see text). Here  $k_c = 2\pi \times 7/24$  and  $k_s = 2\pi \times 1/3$ . Panel (b): Superfluid fraction  $\rho_s/\rho$  (circles), and ratio between the superfluid responses  $\rho_x/\rho_y$  along the  $x$  horizontal and  $y$  vertical axis (diamonds). Panels (c)-(e): Finite-size scaling of  $S(\mathbf{k})$  and  $\rho_s/\rho$  for  $V/t = 3.7$  [panel (c)],  $4.4$  [panel (d)] and  $6.0$  [panel (e)]. Here same symbols refer to the same observables of panels (a) and (b) while lines are linear fitting functions to our numerical data. Panel (f): Relative energy difference  $\Delta E_{\text{rel}}$  between the SS and IS phases as a function of  $V/t$ . The SS has lower energy where  $\Delta E_{\text{rel}}$  is negative. In panels (a), (b), and (f)  $L = 96$ , in all panels  $T/t = 1/20$ .

includes several lattice sites, thus interpolating between nearest-neighbor and long-range physics, while remaining numerically tractable. We utilize numerically exact quantum Monte-Carlo simulations to study the phase diagram of this system as a function of the interaction strength, finding several novel features: (i) For sufficiently strong interactions, the ground state (GS) is a highly anisotropic, insulating stripe crystal that emerges due to cluster self-assembling in the corresponding classical GS. For intermediate interaction strength, we find a surprising (ii) supersolid-supersolid quantum phase transition that separates an isotropic supersolid state from (iii) a highly anisotropic stripe state. In the latter, superfluidity mostly occurs along horizontal (vertical) stripes and is not suppressed at the supersolid-supersolid transition, while diagonal long-range order is found in the perpendicular direction – reminiscent of the so-called *super-stripe* phase found in lattice-based superconductors [45].

We consider the following extended Hubbard Hamiltonian for hard-core bosons confined to 2D

$$\mathcal{H} = -t \sum_{\langle i,j \rangle} (b_i^\dagger b_j + \text{h.c.}) + V \sum_{i < j; r_{ij} \leq r_c} n_i n_j, \quad (1)$$

where  $b_j$  ( $b_j^\dagger$ ) is the bosonic annihilation (creation) operator on site  $j$ ,  $n_j = b_j^\dagger b_j$ , and  $t$  is the nearest-neighbor hopping energy on a square lattice of spacing  $a$ . In the following  $t$  and  $a$  are taken as units of energy and length, respectively. The last term of Eq. (1) represents the soft-shoulder interaction between bosons with strength  $V$ ,  $r_{ij}$  is the distance between sites  $i$  and  $j$ , with  $r_c$  the inter-

action potential cutoff. In classical physics, this interaction is of interest for soft-matter models of, e.g., colloids [46–48]. In quantum physics, similar interactions can be engineered in clouds of cold Rydberg atoms, by weakly-admixing a Rydberg state to the GS using laser light [49–55]. Here, we choose  $r_c = 2\sqrt{2}a$  for which in the classical limit  $V/t \rightarrow \infty$  each particle tries to establish an avoided square region of total area  $16a^2$  [see Fig. 1(a)]. For density  $\rho = 1/9$  this is indeed possible and the system can arrange into an optimal configuration characterized by zero potential energy by covering the lattice with clusters of type I, see Fig. 1(a). Conversely, for higher densities the classical GS corresponds to the solution of a tiling problem, where tiles are constituted by clusters of particles and holes that are effectively bound together by the repulsive interactions. The number of such clusters, or tiles, increases with increasing particle density. Figure 1(b) shows the three clusters I, II, and III (i.e., the tiles) that appear at low energy for densities  $1/9 < \rho < 1/6$ . Similarly to the 1D case [56, 57], the classical GS can then be built from the exponentially large number of permutations of clusters I-III. This large degeneracy is characteristic of long-range interactions and can in principle constitute an obstacle to the solution of the quantum problem. In the following, we determine the effects of quantum fluctuations on this highly degenerate classical GS by computing the quantum phase diagram for model Eq. (1), for an example density  $\rho = 5/36$ . Our focus is the determination of quantum phases and phase transitions in this system.

We study Hamiltonian Eq. (1) by means of path in-

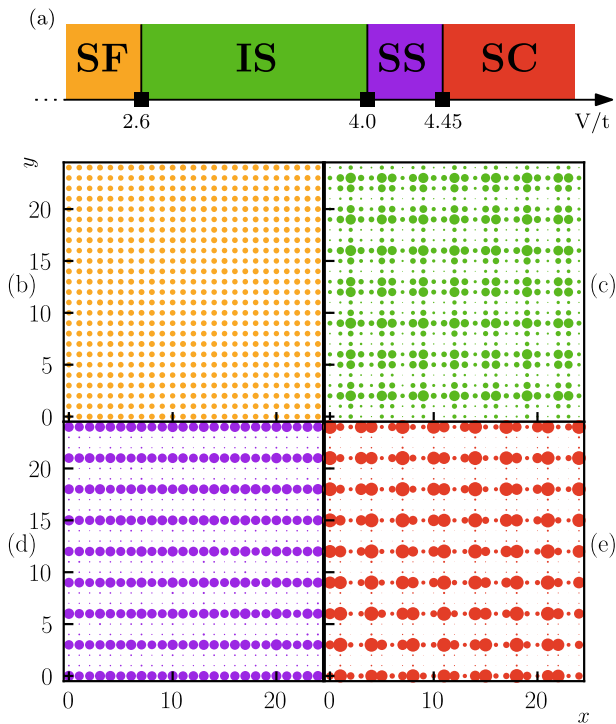


FIG. 3. Ground state (GS) phase diagram of model (1) as a function of the interaction strength  $V/t$  [panel (a)]. For increasing values of  $V/t$  the GS is a superfluid (SF), an isotropic supersolid (IS), an anisotropic stripe supersolid (SS) and stripe crystal (SC) (see text). Panels (b), (c), (d), (e) show site-density maps of a portion of the system for representative interaction strengths at which the GS is a SF ( $V/t = 2.5$ ), IS ( $V/t = 3.7$ ), SS ( $V/t = 4.3$ ), and SC ( $V/t = 6.0$ ), respectively. The size of the dots is proportional to the occupation of the corresponding sites.

tegral Quantum Monte Carlo simulations based on the worm algorithm [58]. This technique is numerically exact for unfrustrated bosonic models, giving access to accurate estimates of fundamental observables such as, e.g., the superfluid fraction  $\rho_s/\rho = \langle W_x^2 + W_y^2 \rangle / (4t\beta\rho)$ , the static structure factor  $S(\mathbf{k}) = \langle \sum_{ij} e^{-i\mathbf{k}\cdot\mathbf{r}_{ij}} n_i n_j \rangle / N^2$ , and the single-particle equal time Green's function  $G(\mathbf{r}) = \langle \sum_i b_i^\dagger b_{i+\mathbf{r}} \rangle / N$ . They measure superfluidity, diagonal long-range, and off-diagonal long-range orders, respectively. Here,  $\beta = 1/(k_B T)$  is the inverse temperature, with  $k_B$  the Boltzmann constant (set to unity);  $W_x$  ( $W_y$ ) is the winding number along the  $x$  ( $y$ ) direction,  $\mathbf{k}$  is a lattice wave vector and  $\langle \dots \rangle$  stands for statistical averaging. Calculations are performed on lattices of size  $N = L \times L$ , with  $L$  as large as  $L = 96$  and temperatures as low as  $T/t = 1/96$ . We find that for  $T/t \leq 1/20$  results are essentially indistinguishable from the extrapolated GS ones.

The main results are presented in Fig. 2. Panels (a) and (b) show estimates of the structure factor  $S(\mathbf{k})$

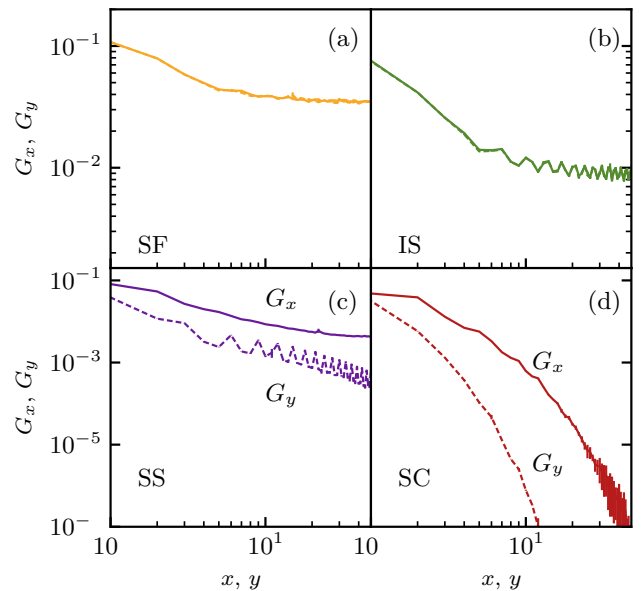


FIG. 4. Green's functions  $G_x$  and  $G_y$  along the  $x$  (solid lines) and  $y$  (dashed lines) directions, respectively, in the SF, IS, SS, and SC. Here  $L = 96$ ,  $T/t = 1/20$  and the values of  $V/t$  are the same as those in Fig. 3(b)-(e).

and the superfluid fraction  $\rho_s/\rho$  (left ordinate axis) together with the ratio between the superfluid responses  $\rho_x/\rho_y \equiv \langle W_x^2 \rangle / \langle W_y^2 \rangle$  along the horizontal and vertical directions (right ordinate axis) as a function of  $V/t$ , for  $T/t = 1/20$  and  $N = 96 \times 96$ , respectively. Examples of finite-size scalings [panels (c)-(e) of the same figure] clarify that the chosen system size is large enough to provide an accurate description of the various observables in the thermodynamic limit, as results obtained for  $L = 96$  essentially coincide with the extrapolated estimates. The combination of  $S(\mathbf{k})$ ,  $\rho_s/\rho$ , and their anisotropies allows for the determination of the quantum phases.

We find that for weak interaction strengths  $V/t \lesssim 2.6$  the GS is a homogeneous superfluid (SF) with  $\rho_s/\rho > 0$ ,  $\rho_x \simeq \rho_y$ , and  $S(\mathbf{k}) = 0$ . For  $2.6 \lesssim V/t \lesssim 4.45$ , however, both the superfluid fraction and the structure factor are finite, indicating the presence of a supersolid GS. Surprisingly, in this range of interaction strength we find two distinct supersolids. Specifically, an isotropic supersolid (IS) and an anisotropic stripe supersolid (SS) occur for  $2.6 \lesssim V/t \lesssim 4.0$  and  $4.0 \lesssim V/t \lesssim 4.45$ , respectively. Within the IS phase,  $S(\mathbf{k})$  [Fig. 2(a)] takes its maximum value for  $\mathbf{k} = (0, \pm k_c)$  and  $(\pm k_c, 0)$  (down- and up-pointing triangles, respectively) with  $k_c = 2\pi \times 7/24$ ; in IS the superfluid response is isotropic [Fig. 2(b), diamonds]. In contrast, in the SS phase the diagonal long-range order is found along one direction only (i.e., the  $y$  direction in the figure), being drastically suppressed along the perpendicular one; in addition, the maximum of the structure factor is found for  $\mathbf{k} = (0, \pm k_s)$ , with

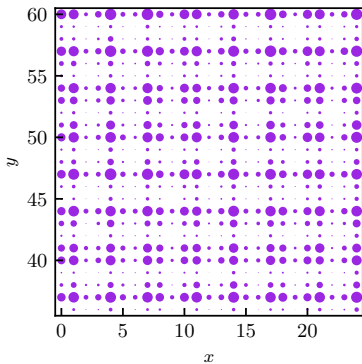


FIG. 5. Out-of-equilibrium density snapshot for a system with  $L = 96$ ,  $V/t = 4.1$  after a quench down to target temperature  $T/t = 1/20$ . For this choice of parameters the corresponding equilibrium phase is a SS. The size of the dots is proportional to the averaged occupation of the corresponding sites.

$k_s = 2\pi \times 1/3 \neq k_c$ , while  $S(0, \pm k_c) = S(\pm k_c, 0) = 0$  [Fig. 2(a), triangles]. Here, the superfluid response becomes strongly anisotropic with  $\rho_x \gg \rho_y$ , signalling the formation of superfluid stripes along the  $x$ -axis. This corresponds to a transition to a self-assembled array of essentially one-dimensional superfluids, which, unexpectedly, have larger superfluid density near the phase boundary:  $\rho_s/\rho$  initially increases within the SS phase, before decreasing again, with increasing  $V/t$ .

Finally, for  $V/t \gtrsim 4.45$  the system loses its superfluid character and, although the maximum value of  $S(\mathbf{k})$  still occurs for  $\mathbf{k} = (0, \pm k_s)$ , secondary peaks emerge at  $\mathbf{k} = (\pm k_c, 0)$ . These latter peaks imply both crystallization along the stripe direction as well as the emergence of weak correlations between particles across different stripes (see below). The resulting GS is a normal crystal.

We find that different metastable states with entirely different quantum orders compete in the region of intermediate strengths of interactions  $V/t \gtrsim 3.0$ . In order to determine the GS we perform two sets of simulations: namely, starting from the equilibrium configuration at  $V_1/t = 3.7$  ( $V_2/t = 5.0$ ) a careful annealing in the interaction strength is performed with annealing step  $0 < \Delta V_1/t \leq 0.1$  ( $-0.1 \leq \Delta V_2/t < 0$ ). When the desired target value of  $V/t$  is reached the calculation leading to a lower energy  $E$  is taken as the GS. Figure 2(f) shows the relative energy difference  $\Delta E_{rel} = (E_2 - E_1)/E_1$  as a function of  $V/t$ . The change in sign at  $V/t \simeq 4.0$  signals the phase transition between the IS and SS phases. The corresponding sudden changes in crystalline order, measured by discontinuities of the structure factors in Fig. 2(a), are consistent with a first order phase transition between the two supersolids.

The formation of stripes remains favored for larger  $V/t$ : hence, the phase transition from the SS to the stripe

crystal phase at  $V/t \simeq 4.45$  is resolved by monitoring the vanishing of superfluidity fraction.

The GS phase diagram of model (1) is summarized in Fig. 3. The demonstration of the existence of novel superfluid and insulating stripe crystals, as well as an exotic supersolid-supersolid quantum phase transitions due to classical cluster formation in a rather general model with a simple isotropic interaction are the main results of this work. Further insight into the discussed ground states can be obtained from the density maps in Fig. 3(b)-(e) and the corresponding Green's function  $G_x$  ( $G_y$ ) along the  $x$  ( $y$ ) axis [Fig. 4]. As expected, for small  $V/t$  (where the system is a homogeneous SF) the average occupation number at each site equals the density  $\rho$  [Fig. 3(b)]. Similarly, the Green's functions (GF) are equal in the  $x$  and  $y$  directions at all distances (i.e.,  $G_x \simeq G_y$ ), within the statistical error bars. They become nearly flat at large distances, which is consistent with the presence of off-diagonal (quasi) long-range order [Fig. 4(a)]. In the IS phase [Fig. 3(c)] the isotropic ordered structure formed by clusters of particles coexists with quantum exchanges and superfluidity. Here,  $G_{x,y}$  displays a weak power-law decay, indicating off-diagonal quasi-long-range order, accompanied by oscillations [Fig. 4(b)], which we find to have a periodicity consistent with particle exchanges between different clusters, thus identifying the underlying classical structure. When stripes are formed in the SS phase, Fig. 3(d), no density modulations appear along their direction (i.e., the horizontal one).  $G_x$  is found to decay as a power-law [Fig. 4(c)], consistent with the measured finite superfluidity along the stripe direction. Long exchange cycles of identical particles take place almost exclusively along the stripes, being strongly suppressed in the perpendicular direction. The overall picture here is that of a 2D quantum system of quasi 1D superfluids (i.e. the stripes). In the SC phase the emergence of a nearly classical cluster-crystalline structure is evident [Fig. 3(e)]. Here long quantum exchanges are completely suppressed and clusters (and particles) can only slightly fluctuate around their equilibrium position due to zero point motion, implying an exponential decay of the GF's in Fig. 4(d), albeit with different slopes in the  $x$  and  $y$  directions.

We find that the phases above are robust for density variations within the range  $1/9 < \rho < 1/6$ , where clusters I-III appear at low energy for large  $V/t$ . In the Supplementary Material [59] we demonstrate that they also persist for  $\rho = 1/6$ , where only clusters of type II and III exist for strong interactions, albeit with a different cluster periodicity (i.e. different  $k_c$ ).

Finally, to exemplify possible out-of-equilibrium scenarios that can emerge with imperfect annealing, Fig. 5

shows a density snapshot obtained when the system is driven away from equilibrium via a temperature quench. Here the target temperature is  $T/t = 1/20$  for a value of  $V/t$  at which the equilibrium phase is a SS. The resulting snapshot is isotropic rather than anisotropic with a crystalline structure similar to panel (c) in Fig. 3, where diagonal long-range order is found for characteristic wave vectors  $\mathbf{k} = (0, \pm k^*)$  and  $(\pm k^*, 0)$  with  $k^* \neq k_c, k_s$ , and the value of  $\rho_s/\rho$  is much smaller than the equilibrium one.

Increasing  $r_c$  or smoothening the edges of the interactions can effectively result in the inclusion of more sites in the interaction volume [59]. This can change the number and type of clusters that appear at low-energy, and thus the resulting crystal structures. For example, for a larger  $r_c = 3a$  and  $\rho = 1/7$  the strong-coupling phase is a SC not oriented in the  $x$  or  $y$ -directions. In these cases, we find that annealing can become increasingly difficult as equilibration is often dominated by the presence of many metastable states, typical of long-range models. A detailed investigation of metastability for model (1) is presented in [60].

We have demonstrated that stripe supersolid and crystals may be realized in the ground state of bosonic, frustration-free cluster-forming Hamiltonians. In particular, for intermediate interaction strength the competition between quantum fluctuations and cluster formation gives rise to a novel supersolid-supersolid transition between an isotropic cluster supersolid and an anisotropic stripe supersolid. These results exemplify the complexities of the determination of quantum phase diagrams of systems with long-range interactions, in a regime where calculations are still feasible. Intriguing out-of-equilibrium scenarios may also emerge and will be the subject of future investigations [60]. Our predictions should be of direct interest for experiments with cold Rydberg-dressed atoms in an optical lattice [61, 62]. More generally, they constitute a step towards the understanding of how long-range interactions can affect the properties of ultracold gases.

*Acknowledgments* – We are grateful to Marcello Dalmonde, Tao Ying, and Peter Zoller for many insightful discussions. Work in Strasbourg was supported by the ERC St-Grant ColDSIM (No. 307688), ANR-ERANET QuantERA - Projet RouTe (ANR-18-QUAN-0005-01), and additional ANR-FWF grant BLUESHIELD. A. A. acknowledges partial support by the ERC under Grant No. 758329 (AGEnTh). F. M. acknowledges support from Fédération de Recherche André Marie Ampère (FRAMA). N. P. acknowledges support from the MURI Program Advanced quantum materials a new frontier for ultracold atoms from AFOSR and the National Science Foundation under the Grant No. DMR-1720465. Computing time provided by HPC-UdS.

*Note added* – After the acceptance of this work, we

became aware of a recent study [63] showing transitions between supersolid phases in a different model. However, as in previous cases (see e.g. [64]), the mechanism behind the transition is a change in density, rather than cluster formation induced by the interaction potential at fixed density.

- 
- [1] A. Campa, T. Dauxois, D. Fanelli, and S. Ruffo, *Physics of Long-Range Interacting Systems* (Oxford University Press, Oxford, New York, 2014).
  - [2] M. Kastner, *Phys. Rev. Lett.* **104**, 240403 (2010).
  - [3] M. Kastner, *Phys. Rev. Lett.* **106**, 130601 (2011).
  - [4] T. Lahaye, C. Menotti, L. Santos, M. Lewenstein, and T. Pfau, *Rep. Prog. Phys.* **72**, 126401 (2009).
  - [5] M. A. Baranov, M. Dalmonte, G. Pupillo, and P. Zoller, *Chem. Rev.* **112**, 5012 (2012).
  - [6] M. Schmitt, M. Wenzel, F. Böttcher, I. Ferrier-Barbut, and T. Pfau, *Nature* **539**, 259 (2016).
  - [7] L. Chomaz, R. M. W. van Bijnen, D. Petter, G. Faraoni, S. Baier, J. H. Becher, M. J. Mark, F. Wächtler, L. Santos, and F. Ferlaino, *Nature Physics* **14**, 442 (2018).
  - [8] V. D. Vaidya, Y. Guo, R. M. Kroeze, K. E. Ballantine, A. J. Kollár, J. Keeling, and B. L. Lev, *Phys. Rev. X* **8**, 011002 (2018).
  - [9] S. Lepoutre, L. Gabardos, K. Kechadi, P. Pedri, O. Gorceix, E. Maréchal, L. Vernac, and B. Laburthe-Tolra, *Phys. Rev. Lett.* **121**, 013201 (2018).
  - [10] E. Lucioni, L. Tanzi, A. Fregosi, J. Catani, S. Gozzini, M. Inguscio, A. Fioretti, C. Gabbanini, and G. Modugno, *Phys. Rev. A* **97**, 060701(R) (2018).
  - [11] L. D. Carr, D. DeMille, R. V. Krems, and J. Ye, *New J. Phys.* **11**, 055049 (2009).
  - [12] D. S. Jin and J. Ye, *Chem. Rev.* **112**, 4801 (2012).
  - [13] M. Saffman, T. G. Walker, and K. Mølmer, *Rev. Mod. Phys.* **82**, 2313 (2010).
  - [14] R. Lw, H. Weimer, J. Nipper, J. B. Balewski, B. Butscher, H. P. Bchler, and T. Pfau, *J. Phys. B: At. Mol. Opt. Phys.* **45**, 113001 (2012).
  - [15] J. W. Britton, B. C. Sawyer, A. C. Keith, C. C. J. Wang, J. K. Freericks, H. Uys, M. J. Biercuk, and J. J. Bollinger, *Nature* **484**, 489 (2012).
  - [16] A. Bermudez, T. Schaetz, and M. B. Plenio, *Phys. Rev. Lett.* **110**, 110502 (2013).
  - [17] P. Richerme, Z.-X. Gong, A. Lee, C. Senko, J. Smith, M. Foss-Feig, S. Michalakis, A. V. Gorshkov, and C. Monroe, *Nature* **511**, 198 (2014).
  - [18] P. Jurcevic, B. P. Lanyon, P. Hauke, C. Hempel, P. Zoller, R. Blatt, and C. F. Roos, *Nature* **511**, 202 (2014).
  - [19] S. John and J. Wang, *Phys. Rev. Lett.* **64**, 2418 (1990).
  - [20] C. Schneider, D. Porras, and T. Schaetz, *Rep. Prog. Phys.* **75**, 024401 (2012).
  - [21] E. Shahmoon and G. Kurizki, *Phys. Rev. A* **87**, 033831 (2013).
  - [22] H. Ritsch, P. Domokos, F. Brennecke, and T. Esslinger, *Rev. Mod. Phys.* **85**, 553 (2013).
  - [23] Y. Tang, W. Kao, K.-Y. Li, and B. L. Lev, *Phys. Rev. Lett.* **120**, 230401 (2018).
  - [24] J. S. Douglas, H. Habibian, C. L. Hung, A. V. Gorshkov, H. J. Kimble, and D. E. Chang, *Nature Photonics* **9**, 326 (2015).

- [25] C. Menotti, C. Trefzger, and M. Lewenstein, *Phys. Rev. Lett.* **98**, 235301 (2007).
- [26] C. Trefzger, C. Menotti, and M. Lewenstein, *Phys. Rev. A* **78**, 043604 (2008).
- [27] P. Bak and R. Bruinsma, *Phys. Rev. Lett.* **49**, 249 (1982).
- [28] F. J. Burnell, M. M. Parish, N. R. Cooper, and S. L. Sondhi, *Phys. Rev. B* **80**, 174519 (2009).
- [29] B. Capogrosso-Sansone, C. Trefzger, M. Lewenstein, P. Zoller, and G. Pupillo, *Phys. Rev. Lett.* **104**, 125301 (2010).
- [30] L. Pollet, J. D. Picon, H. P. Büchler, and M. Troyer, *Phys. Rev. Lett.* **104**, 125302 (2010).
- [31] Y. Li, G. I. Martone, L. P. Pitaevskii, and S. Stringari, *Phys. Rev. Lett.* **110**, 235302 (2013).
- [32] W. Cong-Jun, I. Mondragon-Shem, and Z. Xiang-Fa, *Chinese Phys. Lett.* **28**, 097102 (2011).
- [33] T.-L. Ho and S. Zhang, *Phys. Rev. Lett.* **107**, 150403 (2011).
- [34] C. Wang, C. Gao, C.-M. Jian, and H. Zhai, *Phys. Rev. Lett.* **105**, 160403 (2010).
- [35] J.-R. Li, J. Lee, W. Huang, S. Burchesky, B. Shteynas, F. C. Top, A. O. Jamison, and W. Ketterle, *Nature* **543**, 91 (2017).
- [36] H. Kadau, M. Schmitt, M. Wenzel, C. Wink, T. Maier, I. Ferrier-Barbut, and T. Pfau, *Nature* **530**, 194 (2016).
- [37] I. Ferrier-Barbut, H. Kadau, M. Schmitt, M. Wenzel, and T. Pfau, *Phys. Rev. Lett.* **116**, 215301 (2016).
- [38] L. Chomaz, S. Baier, D. Petter, M. J. Mark, F. Wächtler, L. Santos, and F. Ferlaino, *Phys. Rev. X* **6**, 041039 (2016).
- [39] F. Wächtler and L. Santos, *Phys. Rev. A* **93**, 061603(R) (2016).
- [40] D. Baillie, R. M. Wilson, R. N. Bisset, and P. B. Blakie, *Phys. Rev. A* **94**, 021602(R) (2016).
- [41] A. Macia, D. Hufnagl, F. Mazzanti, J. Boronat, and R. E. Zillich, *Phys. Rev. Lett.* **109**, 235307 (2012).
- [42] R. Bombin, J. Boronat, and F. Mazzanti, *Phys. Rev. Lett.* **119**, 250402 (2017).
- [43] G. G. Batrouni and R. T. Scalettar, *Phys. Rev. Lett.* **84**, 1599 (2000).
- [44] M. Boninsegni and N. V. Prokof'ev, *Rev. Mod. Phys.* **84**, 759 (2012).
- [45] A. Bianconi, D. Innocenti, and G. Campi, *J. Supercond. Nov. Magn.* **26**, 2585 (2013).
- [46] B. M. Mladek, D. Gottwald, G. Kahl, M. Neumann, and C. N. Likos, *Phys. Rev. Lett.* **96**, 045701 (2006).
- [47] D. A. Lenz, R. Blaak, C. N. Likos, and B. M. Mladek, *Phys. Rev. Lett.* **109**, 228301 (2012).
- [48] F. Sciortino and E. Zaccarelli, *Nature* **493**, 30 (2013).
- [49] N. Henkel, R. Nath, and T. Pohl, *Phys. Rev. Lett.* **104**, 195302 (2010).
- [50] G. Pupillo, A. Micheli, M. Boninsegni, I. Lesanovsky, and P. Zoller, *Phys. Rev. Lett.* **104**, 223002 (2010).
- [51] J. E. Johnson and S. L. Rolston, *Phys. Rev. A* **82**, 033412 (2010).
- [52] F. Cinti, P. Jain, M. Boninsegni, A. Micheli, P. Zoller, and G. Pupillo, *Phys. Rev. Lett.* **105**, 135301 (2010).
- [53] J. Honer, H. Weimer, T. Pfau, and H. P. Büchler, *Phys. Rev. Lett.* **105**, 160404 (2010).
- [54] Y.-Y. Jau, A. M. Hankin, T. Keating, I. H. Deutsch, and G. W. Biedermann, *Nature Physics* **12**, 71 (2016).
- [55] J. Zeiher, R. van Bijnen, P. Schauß, S. Hild, J.-y. Choi, T. Pohl, I. Bloch, and C. Gross, *Nature Physics* **12**, 1095 (2016).
- [56] M. Mattioli, M. Dalmonte, W. Lechner, and G. Pupillo, *Phys. Rev. Lett.* **111**, 165302 (2013).
- [57] M. Dalmonte, W. Lechner, Z. Cai, M. Mattioli, A. M. Läuchli, and G. Pupillo, *Phys. Rev. B* **92**, 045106 (2015).
- [58] N. V. Prokof'ev, B. V. Svistunov, and I. S. Tupitsyn, *J. Exp. Theor. Phys.* **87**, 310 (1998).
- [59] See Supplemental Material for discussion on the effects of variations in density and interaction range on the many-body phases presented here, which includes Refs. [52, 55, 65, 66].
- [60] A. Angelone, T. Ying, F. Mezzacapo, G. Masella, M. Dalmonte, and G. Pupillo, arXiv:1606.04267 [cond-mat] (2016), arXiv:1606.04267 [cond-mat].
- [61] H. Schempp, G. Günter, S. Wüster, M. Weidemüller, and S. Whitlock, *Phys. Rev. Lett.* **115**, 093002 (2015).
- [62] T. Boulier, E. Magnan, C. Bracamontes, J. Maslek, E. A. Goldschmidt, J. T. Young, A. V. Gorshkov, S. L. Rolston, and J. V. Porto, *Phys. Rev. A* **96**, 053409 (2017).
- [63] K. Morita and T. Tohyama, *Phys. Rev. B* **99**, 144417 (2019).
- [64] C. Bruder, R. Fazio, and G. Schön, *Phys. Rev. B* **47**, 342 (1993).
- [65] A. W. Glaetzle, M. Dalmonte, R. Nath, C. Gross, I. Bloch, and P. Zoller, *Phys. Rev. Lett.* **114**, 173002 (2015).
- [66] R. van Bijnen and T. Pohl, *Phys. Rev. Lett.* **114**, 243002 (2015).

# Supplementary material of “Supersolid stripe crystal from finite-range interactions on a lattice”

Guido Masella,<sup>1</sup> Adriano Angelone,<sup>2,3</sup> Fabio Mezzacapo,<sup>4,1</sup> Guido Pupillo,<sup>1</sup> and Nikolay V. Prokof'ev<sup>5,1</sup>

<sup>1</sup>*icFRC, IPCMS (UMR 7504) and ISIS (UMR 7006),  
Université de Strasbourg and CNRS, 67000 Strasbourg, France*

<sup>2</sup>*Abdus Salam International Centre for Theoretical Physics, strada Costiera 11, 34151 Trieste, Italy*

<sup>3</sup>*SISSA, via Bonomea 265, 34136 Trieste, Italy*

<sup>4</sup>*Univ Lyon, Ens de Lyon, Univ Claude Bernard,  
CNRS, Laboratoire de Physique, F-69342 Lyon, France*

<sup>5</sup>*Department of Physics, University of Massachusetts, Amherst, Massachusetts 01003, USA*

(Dated: September 20, 2019)

We discuss the effects of variations in density and interaction range on the many-body phases of [S1]. In particular, for a choice of density  $\rho = 1/6$ , we demonstrate the existence of a stripe crystal for large values of interaction strength  $V/t$  and of a quantum phase transition from an anisotropic supersolid to a homogeneous supersolid with decreasing  $V/t$  for Hamiltonian Eq. (1) in the main text [S1].

The numerical results presented in [S1] are obtained for a specific choice of density  $\rho = 5/36$  and for a soft-shoulder interaction potential with range  $r_c = 2\sqrt{2}$ . Below we show that the main quantum phases and phase transitions found in [S1] are robust for density variations within the range  $1/9 < \rho \leq 1/6$ , where clusters of type II and III (in addition to type I) fully determine the crystalline structure for large interaction strengths  $V/t$ , consistent with the discussion in the main text. This is explicitly shown below for the limiting case  $\rho = 1/6$ .

Variations of Hamiltonian terms such as the interaction range  $r_c$  or shape can in principle lead to different crystalline phases at strong coupling with respect to the stripe crystal found in the main text. Below we discuss the crystalline phases occurring by increasing  $r_c$  or by considering a smooth interaction potential instead of the step-like potential of the main text.

## QUANTUM PHASES OF HAMILTONIAN (1) FOR DENSITY $\rho = 1/6$

The phases of Eq. (1) described in the main text for  $\rho = 5/36$  are representative of densities in the range  $1/9 < \rho < 1/6$ , where the clusters of type I, II and III in Fig. 1 dominate the dynamics for a large ratio  $V/t$ . Here, we investigate the case  $\rho = 1/6$ , corresponding to the smallest density increase for which the classical tiling problem has a different structure, as only the clusters of type II and III occur for large  $V/t$ . Calculations are performed for system sizes up to  $N = 96 \times 96$  and temperatures as low as  $T/t = 1/20$ .

The main results are presented in Fig. S1, where, following the definitions found in [S1], the structure factor  $S(\mathbf{k})$  [panel (a)], the superfluid fraction  $\rho_s/\rho$  [panel (b) left ordinate axis], and the ratio between the superfluid responses  $\rho_x/\rho_y$  [panel (b) right ordinate axis] are plotted

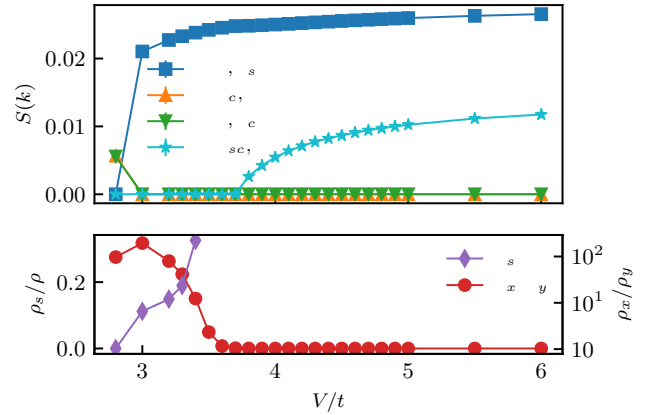


FIG. S1. Panel (a): Structure factor  $S(\mathbf{k})$  as a function of  $V/t$  for values of lattice wave vector  $\mathbf{k} = (k_c, 0)$  (up-pointing triangles),  $(0, k_c)$  (down-pointing triangles),  $(0, k_s)$  (squares),  $(k_{sc}, 0)$  (stars) characteristic of the IS, SS, and SC ordered phase, respectively (see text). Here  $k_c = 2\pi \times 7/24$  and  $k_s = 2\pi \times 1/3$ . Panel (b): Superfluid fraction  $\rho_s/\rho$  (circles), and ratio between the superfluid responses  $\rho_x/\rho_y$  along the  $x$  horizontal and  $y$  vertical axis (diamonds). Data taken from calculations with  $N = 96 \times 96$ ,  $\rho = 1/6$ , and  $T/t = 1/20$ .

as a function of  $V/t$ , for  $T/t = 1/20$  and  $N = 96 \times 96$ .

For large enough interaction strengths  $V/t > 3.9$ , we find a stripe crystal (SC) with no superfluidity, similar to the case treated in the main text. However, the peaks in  $S(\mathbf{k})$  occur here for  $\mathbf{k} = (0, \pm k_s)$  and  $\mathbf{k} = (k_{sc}, 0)$ , with  $k_s = 2\pi/3$  and  $k_{sc} = 2\pi/4$ , respectively. The crystalline order appearing on the  $x$ -axis is thus slightly different from that of the SC phase in [S1] ( $k_{sc} \neq k_c = 2\pi \times 7/24$ ).

Similarly to the main text, by decreasing the interaction strengths we first find an anisotropic stripe supersolid (SS) and then an isotropic supersolid (IS) phase. The latter phases occur for interaction strengths  $3.0 \lesssim V/t \lesssim 3.9$  and  $V/t \lesssim 3$ , respectively. The peaks

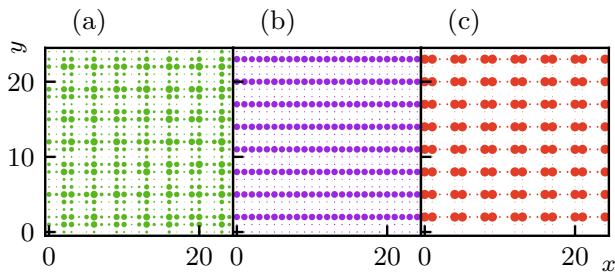


FIG. S2. Site-density maps of a portion of the system for representative interaction strengths at which the ground state is a IS ( $V/t = 2.8$ ) [panel (a)], SS ( $V/t = 3.2$ ) [panel (b)], and SC ( $V/t = 6.0$ ) [panel (c)]. The size of the dots is proportional to the occupation number of the corresponding lattice site. The data is taken from calculations at  $T/t = 1/20$ ,  $\rho = 1/6$ , and  $N = 96 \times 96$ .

in the structure factor within the IS phase are at  $\mathbf{k} = (\pm k_c, 0)$  and  $\mathbf{k} = (0, \pm k_c)$ , identical to the case  $\rho = 5/36$  discussed in the main text.

Further insight can be obtained from the density maps in Fig. S2. In particular, panel (c) shows that for large  $V/t$  in the classical regime the ground state corresponds to a perfect crystalline tiling of the surface with just one single kind of clusters (i.e., cluster II in the  $x$ -direction in the figure). This results in a SC that is qualitatively similar to the one of [S1], albeit with a slightly different periodicity in the  $x$ -direction, as discussed above. By decreasing  $V/t$ , a melting of this crystalline phase gives way to the SS and then IS phases.

In conclusion, we find that the main results discussed in [S1], namely the appearance of an anisotropic (stripe) supersolid and a transition between two different supersolids (IS and SS), are robust against different choices of density in the range  $1/9 < \rho \leq 1/6$ , as long as the strong-coupling low-energy physics is dominated by clusters of the type II and III in Fig. 1, as expected. Further increasing densities with  $\rho > 1/6$  introduces different kinds of clusters in the classical ground state that alter both the strong-coupling stripe crystalline structure, and the ensuing supersolid phases for intermediate values of  $V/t$ . The corresponding quantum phases have then to be investigated on a case-by-case basis, for each density.

### EFFECTS OF THE INTERACTION RANGE AND SHAPE ON THE CRYSTAL PHASES OF EQ. (1)

Varying the interaction range  $r_c$  in Eq. (1) can change the number and shape of relevant clusters in the large  $V/t$  limit. As a consequence, the many-body ground state can change from the predictions of [S1]. As an

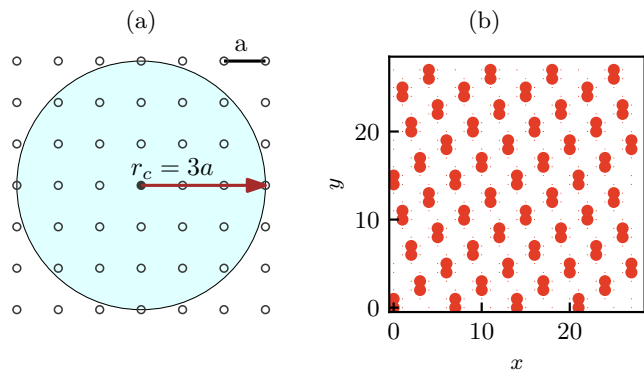


FIG. S3. Panel (a): Interaction volume corresponding to the model Eq. (1) with the cutoff radius of the interaction being  $r_c = 3.0$ . Panel (b): Site-density map of a system with  $N = 28 \times 28$  showing a possible anisotropic crystalline structure forming for the choice  $r_c = 3.0$ . The size of the dots is proportional to the occupation number of the corresponding lattice site. The data is taken from calculations at  $T/t = 1/20$  and  $V/t = 6.0$  at the fixed density  $\rho = 1/7$ .

example, Fig. S3(b) shows a site-density map of a normal (not superfluid) crystalline phase appearing at  $V/t = 6$  for a choice of interaction range  $r_c = 3.0$  and density  $\rho = 1/7$ . The stripe crystal structure is now found to point in a diagonal direction. Further increasing  $r_c$  to large values  $r_c/a \gg 1$  progressively reduces the stripe anisotropy, in favor of a triangular cluster crystal, similar to the continuous case [S2].

Similar effects can be obtained by considering a smoother potential, instead of the stepwise potential of Eq. (1). As an example, Fig. S4 shows results for a potential of the type  $V/[1 + (r/r_c)^\alpha]$ , for different values of  $\alpha$  and  $V/t \gg 1$ . For  $\alpha \rightarrow \infty$  the shape of this interaction approximates well the one in Eq. (1). We find that for  $\alpha \gtrsim 10$  stripe order is favoured along the  $x$ -direction ( $y$ -direction) for  $V/t \gg 1$ , similar to the discussion for Eq. (1). For  $\alpha \lesssim 10$ , however, the stripes progressively give way to a more isotropic, triangular crystalline structure. In particular, for  $\alpha = 6$  (relevant for Rydberg dressed atoms) the density map [panel (c)] and structure factor [panel (f)] indicate a triangular crystal structure that is essentially isotropic in the  $x$  and  $y$  directions. This can be qualitatively explained by considering that lower values of  $\alpha$  effectively include more sites to the edges of the interaction volume for each particle, different from the case of [S1]. [S3]

We find that strong metastable effects are often obtained in the numerical simulations for the situations discussed above in the intermediate regime of interactions  $V/t \gtrsim 1$ . The phase diagram has to be investigated on a case-by-case basis.

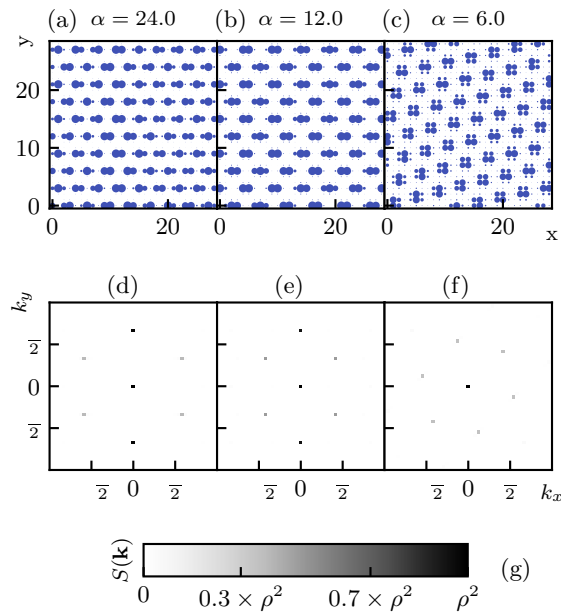


FIG. S4. Panels (a)-(c): site-density maps of a  $48 \times 48$  system for different values of  $\alpha$ . The size of each dot is proportional to the average occupation of the corresponding site. Calculation are performed at  $T/t = 1/20$ ,  $\rho = 5/36$ , and  $V/t = 10, 10, 12$  respectively. Panels (d)-(f): Heatmap plot for the structure factor  $S(\mathbf{k})$  for the same calculations as panels (a)-(c). The intensity-color scale is shown in panel (g).

- 
- [S1] G. Masella, A. Angelone, F. Mezzacapo, G. Pupillo, and N. V. Prokof'ev, *Phys. Rev. Lett.* **123**, 045301 (2019).
  - [S2] F. Cinti, P. Jain, M. Boninsegni, A. Micheli, P. Zoller, and G. Pupillo, *Phys. Rev. Lett.* **105**, 135301 (2010).
  - [S3] We note that for the case of smooth potentials as in Rydberg-dressed gases anisotropy can be re-introduced in the interactions by considering anisotropic Rydberg states (e.g., excited Rydberg  $p$ -type states instead of  $s$  states, as in [S4-S6]).
  - [S4] J. Zeiher, R. van Bijnen, P. Schauß, S. Hild, J.-y. Choi, T. Pohl, I. Bloch, and C. Gross, *Nature Physics* **12**, 1095 (2016).
  - [S5] A. W. Glaetzle, M. Dalmonte, R. Nath, C. Gross, I. Bloch, and P. Zoller, *Phys. Rev. Lett.* **114**, 173002 (2015).
  - [S6] R. van Bijnen and T. Pohl, *Phys. Rev. Lett.* **114**, 243002 (2015).